

# Spectral classification of blue supergiants in M31

David Turban  
Friedrich-Alexander-University  
Erlangen, Germany  
david.turban@physik.stud.uni-erlangen.de

August 21, 2012

## 1 Introduction

Blue supergiants are the visually brightest stars with luminosities reaching up to several  $10^5$  times the solar luminosity. Their masses are in the range of a few tens of solar masses. At the same time, they are enormously large with radii comparable to the Earth's orbit. Because of those features they have been identified as very promising targets for stellar astronomy, enabling quantitative spectral analysis outside the Milky Way [4, 1]. This work adds to these efforts by looking at the closest spiral galaxy, M31 (Andromeda). As a first step for future quantitative studies, high resolution spectra of  $\sim 30$  objects from the NGC 206 association within M31 were classified and placed in a Hertzsprung-Russell diagram.

## 2 Spectral classification

The goal of this process is to sort stars into classes, only taking into account the visual appearance of the spectrum, independently of potentially volatile physical models of the stellar atmosphere. Since the beginning of spectral classification, gradually a now well accepted and well supported scheme has emerged, called the MK system. The MK system has two dimensions, temperature and luminosity. For the temperature sequence the letters O B A F G K M are used, where O is hottest ( $\sim 50000$  K) and M is coolest ( $\sim 3000$  K). Each temperature class is subdivided into subclasses, indicated by a decimal figure (0..9) after the letter. For the luminosity sequence the roman numbers I-V are employed:

- Ia most luminous supergiants
- Ib less luminous supergiants
- II luminous giants
- III normal giants
- IV subgiants
- V main sequence stars (dwarfs)

For this work, only the luminosity class I is relevant. In practice, spectral classification is done by comparing the unknown spectrum visually with spectra of standard stars with known spectral type. Although the classification should not depend on certain physical models as mentioned above, a general understanding of the physics involved in the generation of spectral lines is a very helpful guidance in the process. [3]

### 3 Stellar atmospheres

The atmosphere is the outmost layer of a star from which photons can escape into free space. In this region the observable spectrum is produced. The key physical parameters of the stellar atmosphere are temperature, pressure and the abundances of metals (elements heavier than helium). All strongly influence the appearance of the spectrum. Since no nuclear fusion takes place in the stellar atmosphere, the relevant processes are only absorption and emission of radiation. One defines the absorption coefficient (opacity) caused by a transition between two atomic levels as follows:

$$\kappa(\nu) = n_l \cdot \frac{\pi e^2}{mc} \cdot f_{lu} \cdot \phi(\nu). \quad (1)$$

Here  $n_l$  is the occupation density of the lower level,  $f_{lu}$  the oscillator strength of the transition and  $\phi(\nu)$  a profile function with a maximum at the resonance frequency. Additionally,  $e$  and  $m$  are the charge and mass of the electron respectively and  $c$  is the speed of light. Under the simplifying assumption of local thermodynamic equilibrium (LTE) the occupation numbers are easily calculated using equilibrium thermodynamics. Although LTE is not exactly valid in supergiant atmospheres because of the low densities and the strong radiation field, it still offers a very good qualitative understanding. In LTE the number ratio of two atomic levels of the same ionisation state is just given by the Boltzmann formula, taking into account the statistical weights ( $g_u, g_l$ ) of the excitations:

$$\frac{n_u}{n_l} = \frac{g_u}{g_l} \cdot e^{-(E_u - E_l)/kT}. \quad (2)$$

The other quantities which are involved here are the energies  $E_u$  and  $E_l$  of the upper and lower level of the transition, the Boltzmann constant  $k$  and the temperature  $T$ . The Saha equation on the other hand determines number ratios of successive ionic species:

$$\frac{n_{(i+1)}}{n_{(i)}} = \frac{Z_{(i+1)}}{Z_{(i)}} \frac{1}{n_e} \frac{2(2\pi m k T)^{3/2}}{h^3} \cdot e^{-E_I/kT}. \quad (3)$$

This again contains a Boltzmann factor including the ionisation energy  $E_I$  but in addition also depends on the electron density  $n_e$ . Furthermore,  $Z_i$  and  $Z_{i+1}$  denote the charge numbers of the ions and  $h$  is Planck's constant. It can be concluded that because of their low density, supergiant atmospheres have a larger fraction of ionised atomic states compared to less luminous (and therefore denser) stars of the same surface temperature. Generally, it can be seen from both formulae that the number density of specific atomic or ionic states depends strongly on temperature. Hence, it is explained why stellar spectra show temperature trends of varying line strengths. This ultimately makes it possible to visually arrange spectra in a temperature sequence and justifies the basic assumptions of the MK system.

There are several mechanism that have the effect of broadening spectral lines beyond their natural width. Doppler broadening is a result of the thermal motion of the absorbing atoms and ions in the stellar atmosphere. At the low densities and relatively high temperatures that occur here, the perfect gas is a very good approximation and the particles follow a Maxwell velocity distribution. Hence, Doppler broadening yields a Gaussian line profile. Another mechanism that is particularly important for luminosity classification is pressure broadening via the Stark effect. Absorbing atoms are constantly disturbed by collisions with other atoms in the atmosphere. Their electromagnetic fields interfere with the absorbing atom and modify the energy levels, leading to line broadening. The strength of the effect depends on the frequency of particle collision and hence on the atmospheric pressure. Main sequence dwarfs are relatively compact and therefore they have dense atmospheres with comparatively high pressure. Hence their spectra exhibit significant pressure broadening. As one goes to greater luminosities, the stars become much more extended and have lower atmospheric densities and pressures. Therefore line broadening is less pronounced and especially supergiants show very narrow absorption features. [3]

## 4 Observational data

All spectra were taken with the DEIMOS multi-object spectrograph in combination with the Keck II telescope situated on Mauna Kea, Hawaii. In order to select blue supergiant candidates within NGC 206 suitable for high resolution spectroscopy, B-V photometry was employed. Objects with slightly redder color index were preferred to account for reddening. Since the distribution of reddening is inhomogenous due to varying densities of interstellar gas, it was expected that the selected sample also includes cooler targets. Additional constraints were introduced by the instruments used, in particular the DEIMOS multi-object spectrograph. To achieve a uniform wavelength coverage for all objects, their position with respect to the dispersion direction of the diffraction grating had to be roughly equal. Also, in avoidance of mutual interference of different spectra on the CCD, a vertical minimum gap between the slits was necessary. Eventually, taking into account all the described demands, 74 tar-

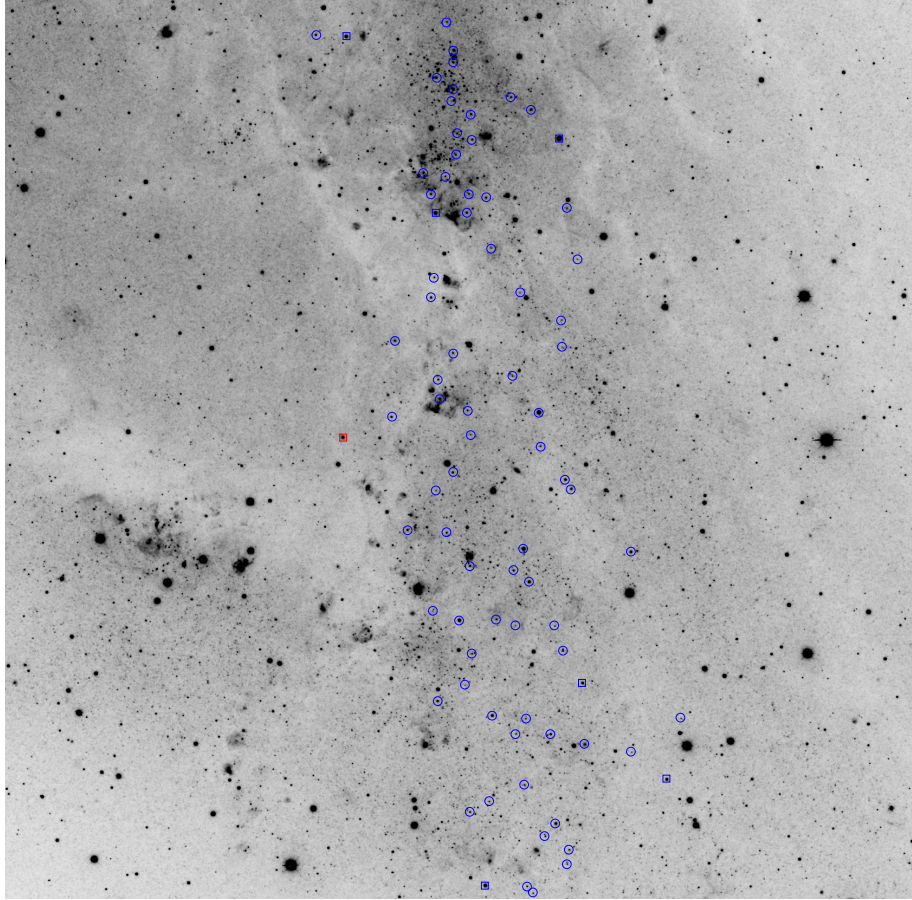


Figure 1: NGC 206 field with marked targets. The targets form a column, such that the horizontal dispersion of the spectra by the DEIMOS spectrograph results in roughly equal wavelength coverage for all objects. The red square indicates the guide star (RA 00:40:37.98 DE 40:39:32.4).

gets were selected for spectroscopy (figure 1). Typical visual brightnesses of the objects are in a range of 16-19 mag.

For spectroscopy a 1200 l/mm grating was used, resulting in a spectral resolution of close to 1 Å in the relevant wavelength region. Four 2700 s exposures were taken in the blue (BAL12 filter) with a center wavelength of 4900 Å, resulting in an approximate coverage of 3800-6200 Å. For the red part of the spectrum (center 7450 Å, GG455 filter), three 1800 s exposures were taken, giving a coverage of roughly 6000-8800 Å. The spectral raw data was reduced employing the DEIMOS reduction pipeline, which involved bias and flatfield correction as well as wavelength calibration. Because of the low sensitivity of the instruments in the 3800-4900 Å range, this spectral window had to be discarded in the further analysis.

## 5 Spectral analysis

A rough visual inspection of the spectra led to a further selection of finally  $\sim 30$  supergiants of approximate types B A (F) for precise spectral analysis, discarding cooler stars, foreground dwarfs and high noise spectra. As a last step of processing before the actual analysis, the selected spectra had to be normalised to make them comparable with references. This was done by spline fitting using 5-10 continuum reference points for each spectral window and then dividing the spectrum by the fit.

Due to the mentioned sensitivity issues in the blue spectral window, the classification procedure had to focus on the visual/red part of the spectrum. Suitable reference spectra were provided by the Indo-U.S. library of Coudé Feed spectra [10]. The spectra offer high resolution of  $\sim 1\text{Å}$  and wide wavelength coverage (3460-9464 Å). Because of the comparable resolution, downgrading of either data or references was unnecessary. For classification an already normalised catalogue taken from the Indo-U.S. library was used, covering the luminosity classes Ia/b and II and the types B0-F5 in steps of 5 subtypes. This enabled a classification within roughly two subtypes uncertainty.

The analysis was done by plotting the catalogue references over the normalised spectra using software tools and visually comparing them. Important spectral features regarded in this process were the Paschen series, the Balmer  $H\alpha$   $\lambda 6563$  line, the O I  $\lambda\lambda 7771-5$  and N I  $\lambda\lambda 8680-6$  triplets as well as Si II  $\lambda\lambda 6371, 6347$ . The width and total number of discernible Paschen lines could be used as a sensitive luminosity indicator. To precisely discriminate temperatures, He I was a crucial indicator (e.g.  $\lambda\lambda 6678, 5876$ ) for early types. For later types the Ca II triplet lines ( $\lambda\lambda 8498, 8542, 8662$ ) served this purpose.

Line trends provided a means of verifying the correctness of the initial classification and identifying potential errors [5]. For that the equivalent widths of the following 10 spectral features were measured and plotted against the spectral type:

O I	7771-5 triplet
H I	8598
He I	5876
He I	6678
Si II	6347
N I	8680-6 triplet
N I	8703
Ca II	8542
Mg I	5184
Fe II	5018

The plots can be found in appendix A. Some of the trends show considerable scatter due to non-uniform metallicities in the target stars and difficulty of precise measurements in the case of line blends. Still, it was possible to identify consistent outliers and revise spectral types accordingly.

## 6 Photometry

The photometric data were taken from [6]. The target objects were matched with the catalogue by their positions. The visual apparent magnitudes provided were then converted into absolute bolometric magnitudes:

$$M_{bol} = m_V - \mu + BC \quad (4)$$

Here  $m_V$  is the visual apparent magnitude from the photometric catalogue and  $\mu$  is the distance modulus to M31 with an employed value of 24.47 [9]. The bolometric correction BC accounts for the fact that only part of the stellar light is emitted in the visual part of the spectrum. Values for BC were taken from [8], according to the previously determined spectral types.

## 7 Results

A table of all relevant data including classification results and photometry is provided in appendix B.

For the Hertzsprung-Russell diagram the absolute bolometric magnitudes were converted into solar luminosities, adopting a value of 4.75 for the absolute bolometric magnitude of the Sun [2]. Also, the determined spectral types were converted into temperatures according to [8]. Figure 2 shows the final HR diagram. For reference, numerical evolution tracks are overplotted, taken from [7]. The tracks cover a mass range of 9-40 solar masses, assuming solar metallicity and no rotation for the numerical simulation. As shown by the HR diagram the investigated objects have masses ranging from 9 solar masses on the lower end up to above 25 solar masses. Their luminosities of  $10^4$ - $10^5$  solar luminosities are also consistent with supergiant stars. Additionally, the positions off the main sequence, developing towards the red supergiant stage, indicate a late evolu-

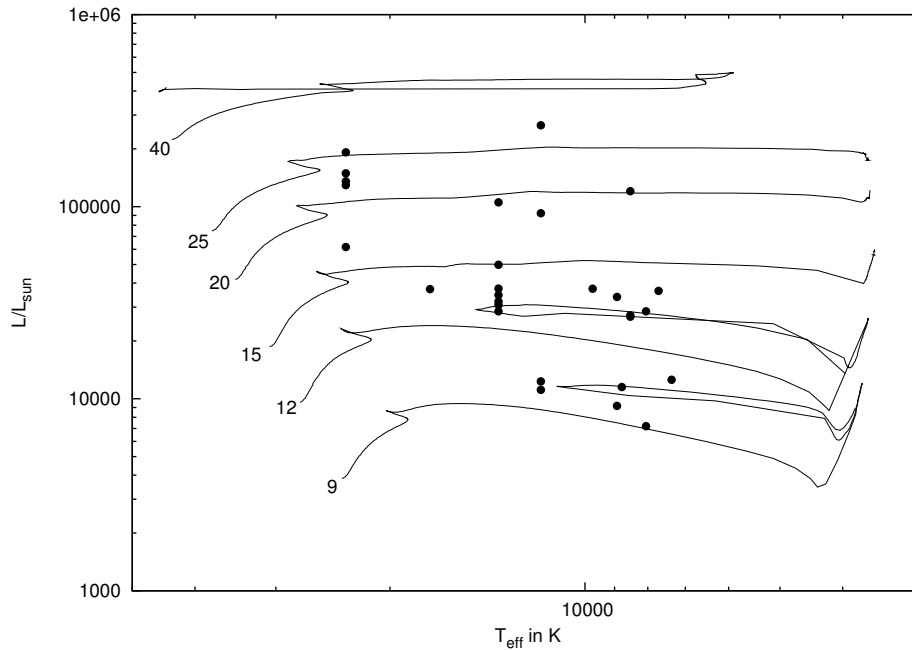


Figure 2: Hertzsprung-Russell diagram of the analysed supergiants with overplotted numerical evolution tracks for model stars with 9-40 solar masses taken from [7].

tionary state with H-shell burning, again compatible with a supergiant nature of the objects.

Figure 3 shows a spectral sequence of selected supergiants from the sample. The temperature trends exhibited by features like  $H\alpha$ , He I or the Ca II and N I triplets are clearly visible.

This project work only encompassed the classification of the NGC 206 spectra as stated before. In a further analysis one could determine the quantitative abundances of elements by comparing the data with numerical spectra based on the obtained classification. This would enable conclusions about the chemical composition of M31.

## 8 Acknowledgements

I would like to warmly acknowledge the great support of my project supervisor Norbert Przybilla. His counsel and expertise was crucial at every stage of this work. Special thanks also go to Uli Heber who was involved in assigning the project, to Veronika Schaffenroth for providing me with the normalised spectral catalogue and to Andreas Irrgang for his help with various ISIS scripts.

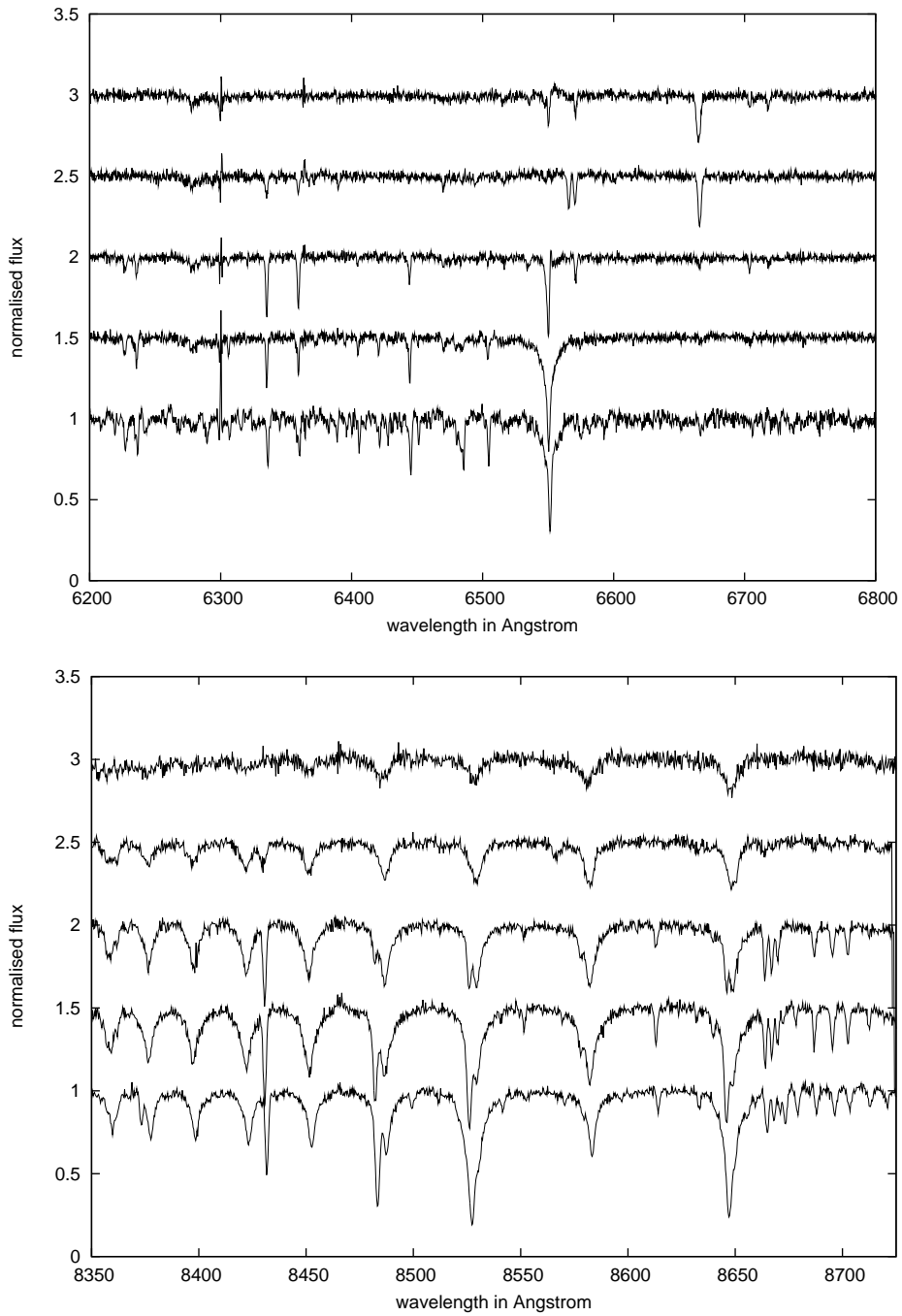
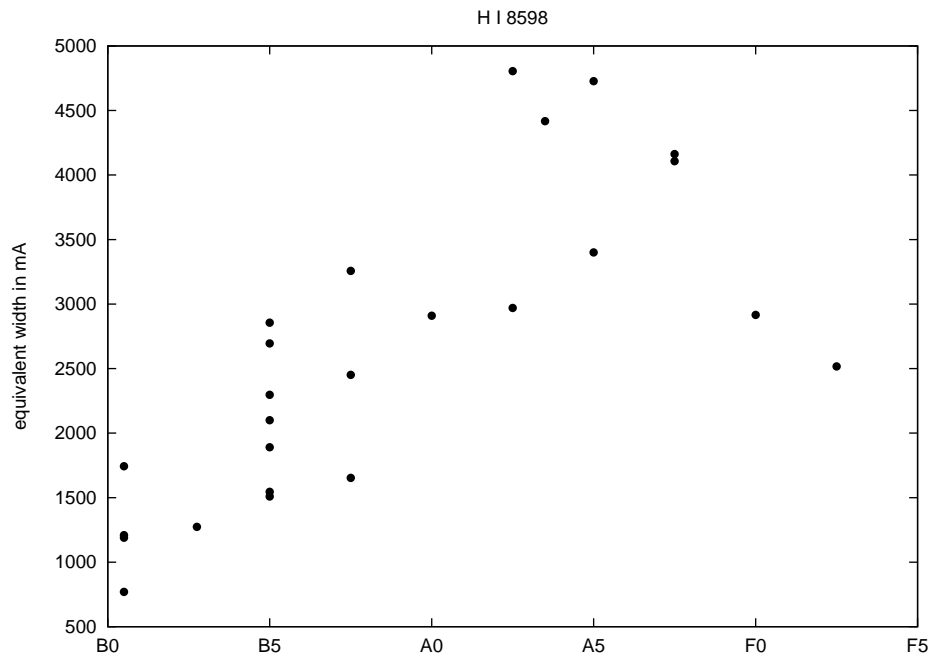
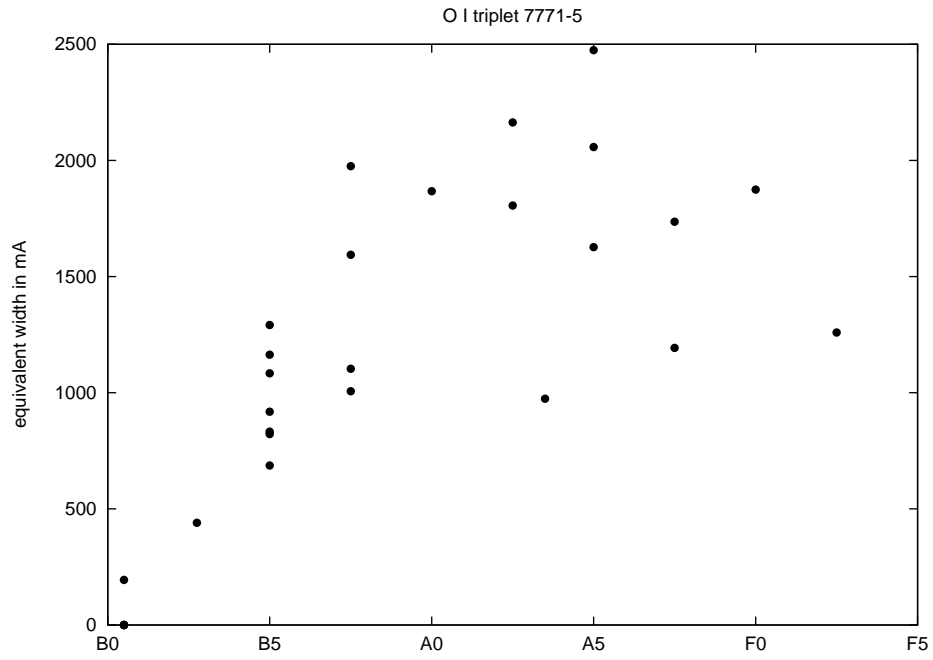


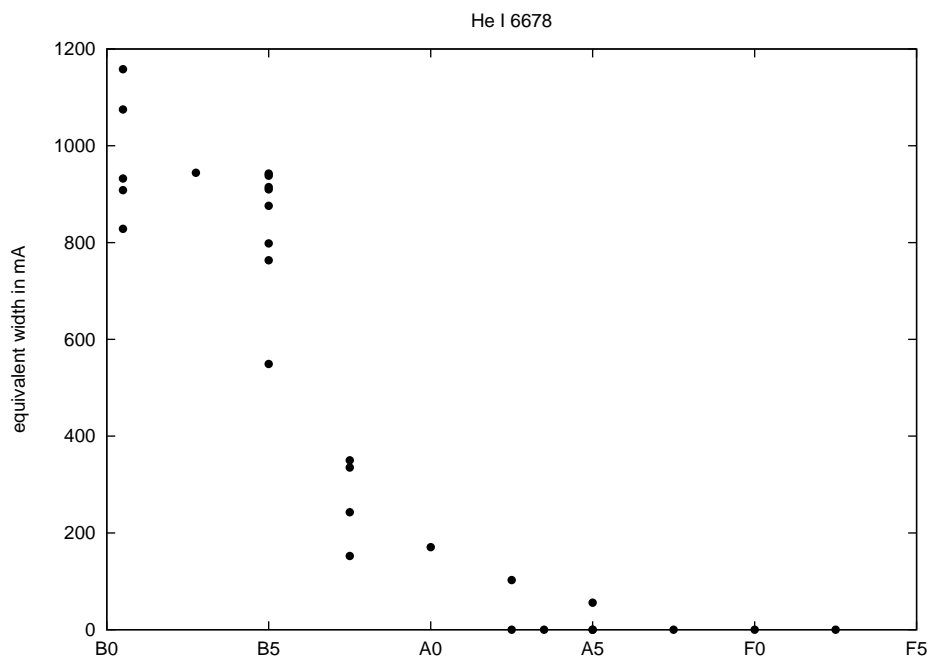
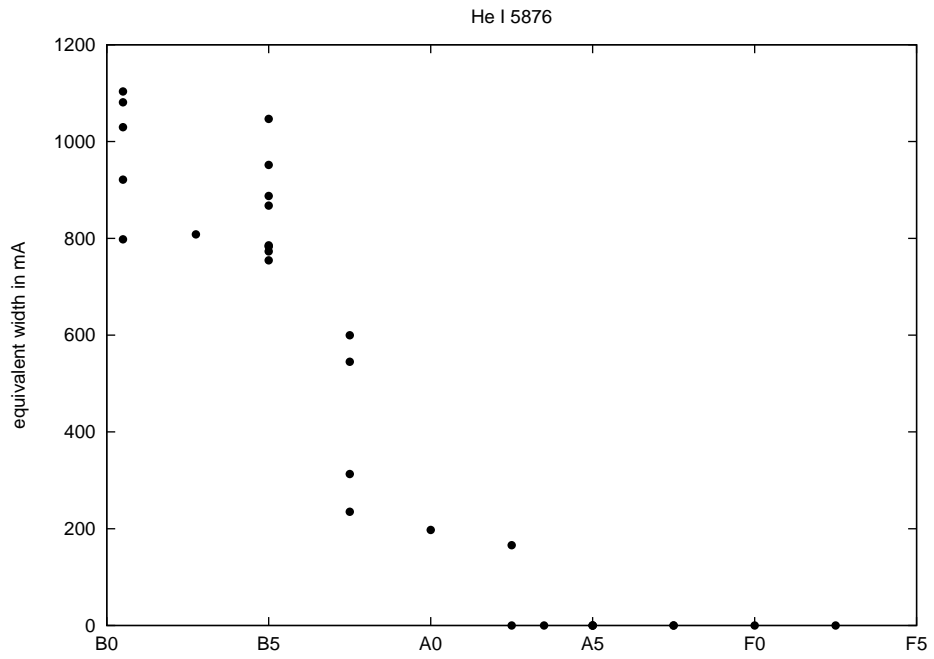
Figure 3: Spectral sequence of supergiants from NGC 206 with approximate types B0, B5, A0, A5 and F0 (top to bottom). Notable line features in the upper panel are  $H\alpha$   $\lambda 6563$ , Si II ( $\lambda\lambda 6347, 6371$ ) and HeI  $6678$ . The lower panel shows part of the Paschen series as well as the Ca II triplet ( $\lambda\lambda 8498, 8542, 8662$ ) and the N I  $\lambda\lambda 8680-6$  triplet, both only visible in the later types.

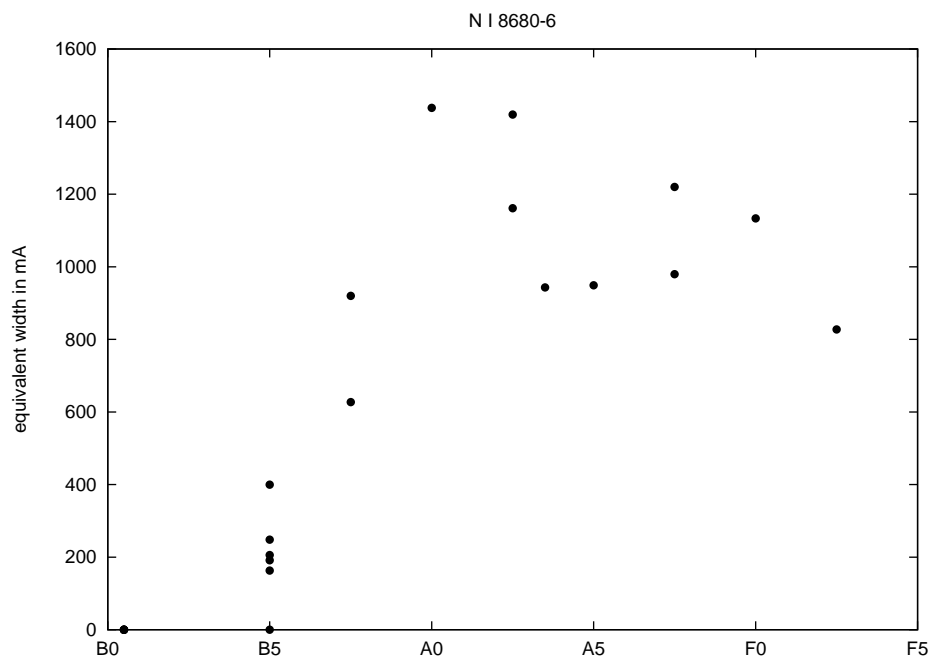
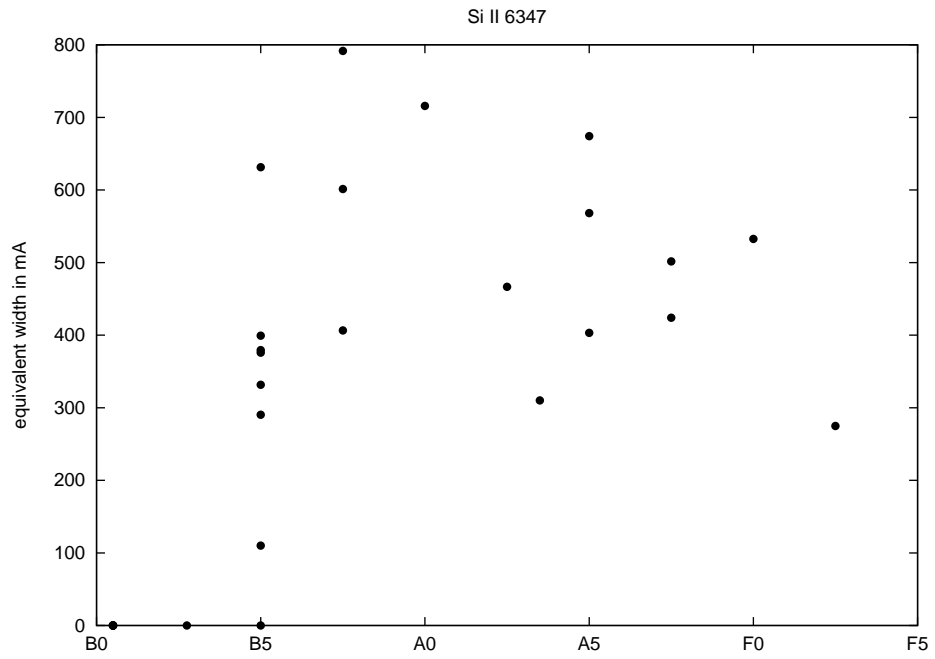
## References

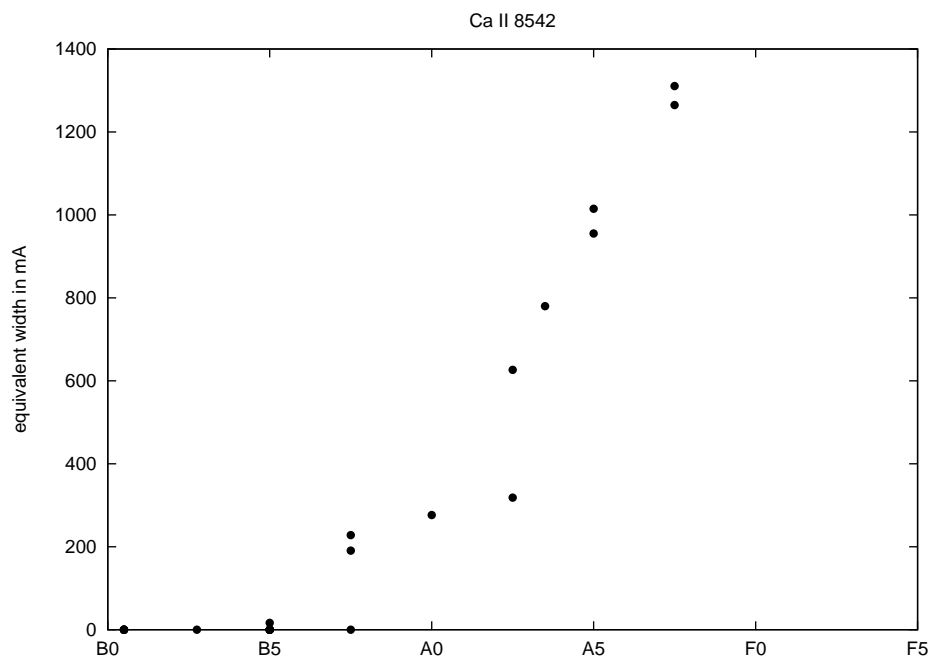
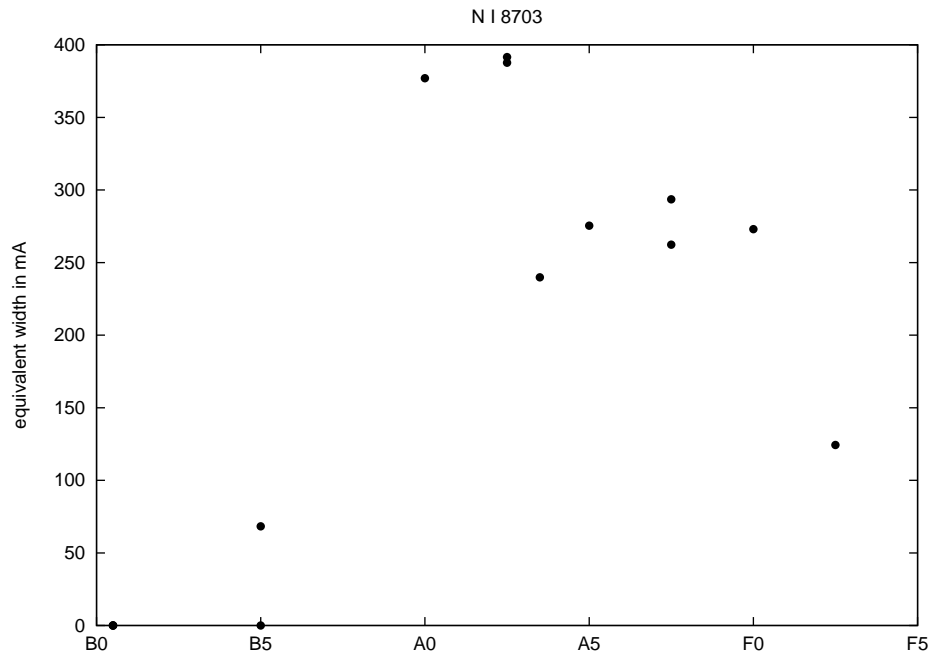
- [1] Fabio Bresolin, Wolfgang Gieren, Rolf-Peter Kudritzki, Grzegorz Pietrzyński, and Norbert Przybilla. Spectroscopy of Blue Supergiants in the Spiral Galaxy NGC 300. *The Astrophysical Journal*, 567(1):277, 2002.
- [2] G. Cayrel de Strobel. Stars resembling the Sun. *Astronomy and Astrophysics Review*, 7:243–288, 1996. 10.1007/s001590050006.
- [3] R.O. Gray, C.J. Corbally, and A.J. Burgasser. *Stellar Spectral Classification*. Princeton Series in Astrophysics. Princeton University Press, 2009.
- [4] Rolf P. Kudritzki, Fabio Bresolin, and Norbert Przybilla. A New Extragalactic Distance Determination Method Using the Flux-weighted Gravity of Late B and Early A Supergiants. *The Astrophysical Journal Letters*, 582(2):L83, 2003.
- [5] D. J. Lennon. Revised spectral types for 64 B-supergiants in the Small Magellanic Cloud: metallicity effects. *Astronomy and Astrophysics*, 317:871–882, February 1997.
- [6] Philip Massey, K. A. G. Olsen, Paul W. Hodge, Shay B. Strong, George H. Jacoby, Wayne Schlingman, and R. C. Smith. A Survey of Local Group Galaxies Currently Forming Stars. I. UBVRI Photometry of Stars in M31 and M33. *The Astronomical Journal*, 131(5):2478, 2006.
- [7] G. Meynet and A. Maeder. Stellar evolution with rotation. X. Wolf-Rayet star populations at solar metallicity. *Astronomy and Astrophysics*, 404:975–990, June 2003.
- [8] K. Schaifers and H. H. Voigt. *Stars and Star Clusters*, volume 2b of *Landolt-Börnstein - Group VI Astronomy and Astrophysics*. Springer-Verlag Berlin Heidelberg, 1982.
- [9] K. Z. Stanek and P. M. Garnavich. Distance to M31 with the Hubble Space Telescope and Hipparcos Red Clump Stars. *The Astrophysical Journal Letters*, 503(2):L131, 1998.
- [10] Francisco Valdes, Ranjan Gupta, James A. Rose, Harinder P. Singh, and David J. Bell. The Indo-US Library of Coudé Feed Stellar Spectra. *The Astrophysical Journal Supplement Series*, 152(2):251, 2004.

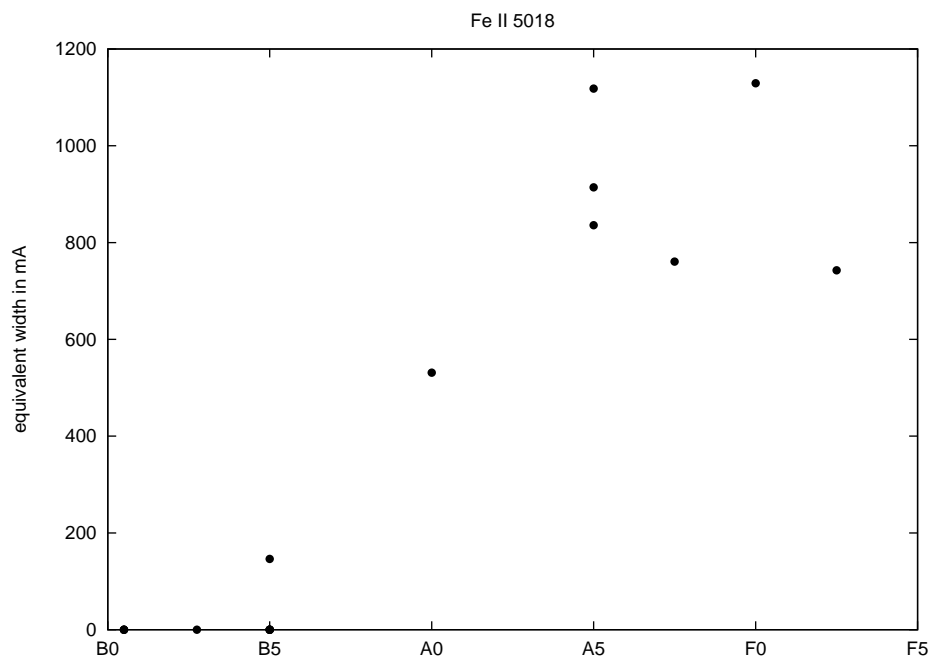
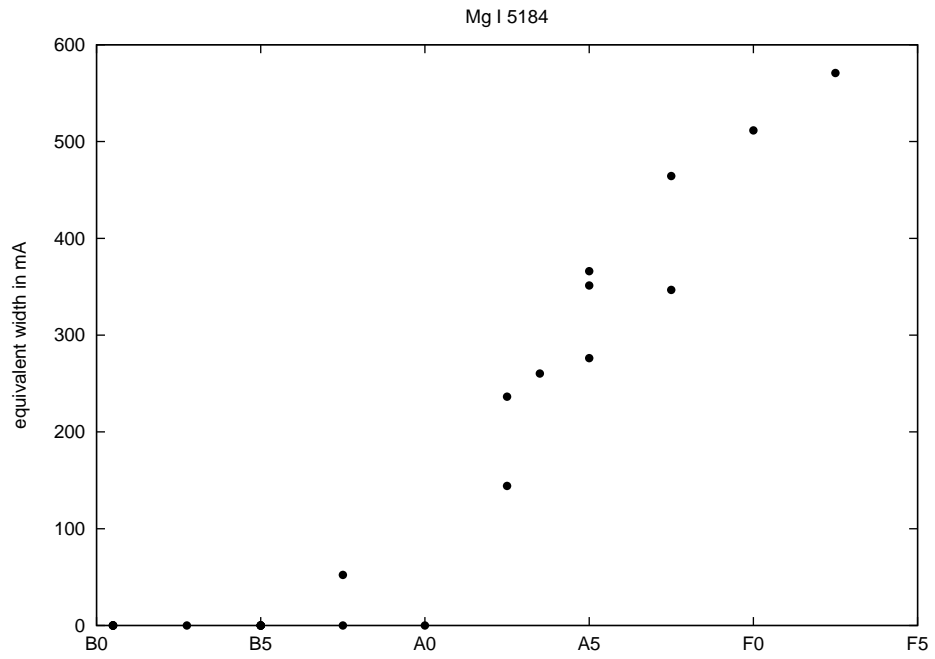
## A Line trends











## B Data

ID	RA	DE	Type	$m_V$	$M_{bol}$
MAG050466	00:40:21.21	40:31:17.1	A5Ia	16.64	-7.95
MAG054663	00:40:13.77	40:32:35.7	A5II-F0II	19.62	-4.89
MAG055664	00:40:21.64	40:32:56.5	F0Ia	17.82	-6.65
MAG055702	00:40:25.02	40:32:57.2	F0Ib-F5Ib	18.98	-5.49
MAG061179	00:40:29.23	40:34:26.6	B0.5Ia-B5Ib	19.21	-6.67
MAG061357	00:40:20.37	40:34:28.8	A5-F0 Ia-Ib	18.43	-6.08
MAG063322	00:40:21.15	40:34:56.5	A2II-A5II	19.27	-5.40
MAG063885	00:40:30.47	40:35:03.8	B5Ia-A0Ia	16.38	-8.81
MAG064737	00:40:33.04	40:35:14.2	B0.5Ia	18.62	-8.03
MAG067779	00:40:25.13	40:35:58.5	A5II	18.26	-6.33
MAG068175	00:40:29.38	40:36:04.2	A5II-F0II	18.12	-6.38
MAG070627	00:40:31.64	40:36:41.3	~B0.5Ib	18.46	-8.18
MAG070817	00:40:35.46	40:36:44.6	A5Iab-Ib	18.28	-6.31
MAG077097	00:40:29.24	40:38:30.1	B5Ib-A0Ib	19.71	-5.47
MAG078570	00:40:29.50	40:38:57.0	~B5Iab	18.73	-6.68
MAG080467	00:40:32.33	40:39:31.5	A0Ia	18.19	-6.68
MAG080632	00:40:25.08	40:39:34.6	A0Ib-A5Ib	19.55	-5.15
MAG089533	00:40:18.68	40:41:44.0	B5Ib-A0Ib	19.82	-5.36
MAG090408	00:40:27.08	40:41:57.2	~B0.5Ia-II	19.42	-7.22
MAG094633	00:40:32.92	40:42:57.7	B0.5Ia	18.19	-8.45
MAG094636	00:40:29.20	40:42:57.7	B5Ib	19.03	-6.38
MAG095882	00:40:31.49	40:43:17.3	B5Ib	18.90	-6.51
MAG096144	00:40:33.61	40:43:21.6	~B5Ia	18.42	-6.99
MAG097413	00:40:30.43	40:43:41.1	~B5Iab-Ib	18.82	-6.60
MAG099069	00:40:30.32	40:44:04.8	B5Ib	18.95	-6.47
MAG100680	00:40:28.92	40:44:26.2	A0Ia-A5Ia	18.14	-6.57
MAG101866	00:40:30.59	40:44:41.7	B5Ib-II	17.61	-7.80
MAG102108	00:40:24.99	40:44:44.7	~B0.5II	18.57	-8.08
MAG106123	00:40:30.56	40:45:37.3	B5Ib-A0Ib	17.52	-7.66